

AAS 03-067



Mars Reconnaissance Orbiter Design Approach for High-Resolution Surface Imaging

S.W. Lee and E.D. Skulsky, NASA/JPL

J. Chapel, D. Cwynar, and R. Gehling, Lockheed Martin Space Systems

A. Delamere, Ball Aerospace and Technologies Corp.

26th ANNUAL AAS GUIDANCE AND CONTROL CONFERENCE

February 5-9, 2003
Breckenridge, Colorado

Sponsored by
Rocky Mountain Section



American Astronautical Society
Rocky Mountain Section

AAS Publications Office, P.O. Box 28130 - San Diego, California 92198

MARS RECONNAISSANCE ORBITER DESIGN APPROACH FOR HIGH-RESOLUTION SURFACE IMAGING

Steven W. Lee,* Eli David Skulsky,* J. Chapel, D. Cwynar,**
R. Gehling,** and A. Delamere†**

The Mars Reconnaissance Orbiter (MRO) will explore Mars equipped with a suite of six scientific instruments and two engineering experiments, and supporting two additional facility investigations. One of the objectives of the MRO mission is to use the High-Resolution Imaging Science Experiment (HiRISE) to provide 50 cm/pixel images of future Mars landing sites. To achieve such detail, MRO must meet some very challenging target-relative pointing and pointing stability requirements. A combination of analysis, operational constraints, and spacecraft design modifications were utilized to ensure that the necessary pointing requirements will be met.

INTRODUCTION

In this paper, we begin by briefly reviewing the ambitious objectives of the Mars Reconnaissance Orbiter (MRO) mission.^{**1} We then discuss the instruments and investigations supported by the mission, and provide a brief overview of the spacecraft. We follow with a more detailed discussion of the High-Resolution Imaging Experiment (HiRISE)—a camera which will provide detailed (50 cm/pixel) images of the Mars surface, and which drives the target-relative pointing and pointing stability requirements for the spacecraft. Next, we describe the MRO Guidance and Control system and present the driving HiRISE target-relative pointing and pointing stability requirements, along with a budgets and allocations for each requirement. In the final section, we identify and describe the disturbance sources and provide a detailed discussion of each along with the analysis approach for pointing stability requirements.

Mission Overview

The Mars Reconnaissance Orbiter (MRO) is a key element in NASA's Mars Exploration Program. MRO will explore Mars for candidate sites where extinct or extant life might be found, contribute to our understanding of Mars' global climate, and provide detailed images of future landing sites. Echoing NASA's "follow the water" strategy,^{**2} the specific objectives of the MRO mission are to:

- Search for sites showing evidence of aqueous and/or hydrothermal activity.
- Map and characterize in detail the stratigraphy, geologic structure and composition of Mars surface features at many globally-distributed targeted sites.
- Provide high-resolution imagery to support the selection of future landing sites.

*Jet Propulsion Laboratory, California Institute of Technology, Pasadena, CA.

**Lockheed Martin Space Systems, Denver, CO.

†Ball Aerospace and Technologies Corp, Boulder, CO.

All correspondence should be sent to Steven W. Lee, Jet Propulsion Laboratory, 4800 Oak Grove Drive, M/S 301-420, Pasadena, CA 91109, e-mail: steven.w.lee@jpl.nasa.gov.

- Recover the Mars Climate Orbiter (MCO) atmosphere and climate science objectives by characterizing Mars' seasonal cycles and diurnal variations of water, dust, and carbon dioxide.
- Detect on Mars the presence of liquid water and determine the distribution of ground ice in the upper surface, particularly within the near-surface regolith.
- Provide atmospheric observations in addition to the MCO capabilities to further define Mars' atmospheric structure and circulation.
- Characterize the Martian gravity field in greater detail to understand better Mars' geologic history and the structure of its crust and lithosphere.
- Provide telecom and/or navigation relay capability to support future Mars orbiter and lander missions.

Mission Synopsis

The Mars Reconnaissance Orbiter will launch in August 2005, and will arrive at Mars in March 2006. Similarly to two previous Mars spacecraft, MRO will use aerobraking^{**3,4} to attain the primary science orbit (PSO), which will have a periapsis altitude near 255 km and an apoapsis altitude near 320 km. The PSO will be sun-synchronous with an ascending node orientation of approximately 3:00 pm local mean solar time (LMST). During the PSO, repetitive (mapping) and targeted observations of the planet's surface and atmosphere will be conducted over a time span of one Martian year (687 Earth days), nominally from November 2006 through November 2008. Throughout the PSP, the orbiter will be oriented with the primary science instruments pointing towards areoedetic nadir. Using slew maneuvers, MRO will provide the capability to image targets up to 30 deg off-nadir. Science data acquisition will be planned such that data can be downlinked to the DSN during two 8-hour tracking passes every day.

The MRO orbiter will also support the Mars Exploration Program by providing approach navigation and relay communications support to various Mars landers and orbiters through its telecommunications/navigation subsystem. During these support periods, relay and navigation functions will have priority over orbiter science observations (including site characterization), although such observations may continue if they do not interfere and are within the mission resources.

Instrument/Investigation Overview

A suite of six science instruments, two engineering payloads, and two facility investigations has been selected to support MRO's objectives:

- High-Resolution Imaging Science Experiment (HiRISE). A 0.5 m aperture, time delay integration (TDI) telescope with 12 m focal length. HiRISE provides very high resolution panchromatic and color images (25 cm/pixel at 255 km). At full resolution, a single HiRISE image is expected to be as large as 16 Gbit. HiRISE will investigate stratigraphy, processes, and site morphology.
- Compact Reconnaissance Imaging Spectrometer for Mars (CRISM). A Ritchey-Chretien-based spectrometer providing high spectral (400 – 4050 nm) and spatial (15 m/pixel at 255 km) images. CRISM will investigate regional and local surface composition and atmospheric properties.
- Context Imager (CTX). A wide swath (> 30 km wide at 255 km orbit altitude) monochromatic telescope with 6 m resolution at 255 km. CTX will investigate regional stratigraphy and morphology in addition to providing context for other, higher resolution investigations.
- Shallow Subsurface RADAR (SHARAD). A 15–25 MHz radar capable of providing 15 m vertical resolution to a depth of 1 km. SHARAD will investigate regional near-surface ground structure including detection of water ice.
- Mars Color Imager (MARCI). A multispectral (5 visible and 2 UV) imager providing 1 – 10 km/pixel nadir resolution, < 7 km limb resolution and a limb-to-limb field of view. MARCI recovers a portion of the MCO science with its global weather and surface change observations.
- Mars Climate Sounder (MCS). A 4 cm aperture, f/1.7 telescopic filter radiometer in nine spectral channels between 0.3 – 30.0 μm. MCS provides nadir and limb scans to investigate atmospheric fields, transport phenomenon, and polar processes.

- Optical Navigation Camera (ONC). An engineering/navigation experiment to validate optical navigation techniques Upon Mars approach, ONC will image Mars, Phobos, Deimos, and background stars for navigation purposes.
- Electra. Electra provides a two-way UHF radio link to future Mars spacecraft for command and telemetry relay. Electra also supports one-way X-band Doppler for future incoming Mars spacecraft.
- Gravity Science facility investigation. Utilizing Doppler data, the gravity science team will develop an improved Mars gravity model and investigate transient mass changes.
- Atmospheric Structure facility investigation. Utilizing accelerometer data obtained during aerobraking drag passes, the atmospheric structure team will investigate upper atmospheric structure and variability.

Spacecraft Overview

The MRO spacecraft is a relatively large spacecraft with exceptional data collection and return capability. Figure 1 shows two views of the MRO spacecraft configuration during the primary science phase. The direction of flight is in the plane of the solar arrays with the instrument deck nominally oriented towards nadir. Total spacecraft wet mass is approximately 2000 kg at launch. Two solar panels provide 20 m^2 of total useable substrate area to generate up to 2880 W of power at Mars. A large (3 m diameter) High Gain Antenna (HGA) supports downlink rates as high as 6 Msps. Both solar arrays and the HGA are mounted on two-axis gimbals to maximize power and communications flexibility while maintaining a nadir body orientation. The spacecraft structure features an open bay design with a nadir-pointed instrument deck. This structure is built around a large, 1187 kg capacity propellant tank, which provides up to 1578 m/s delta-V capability.

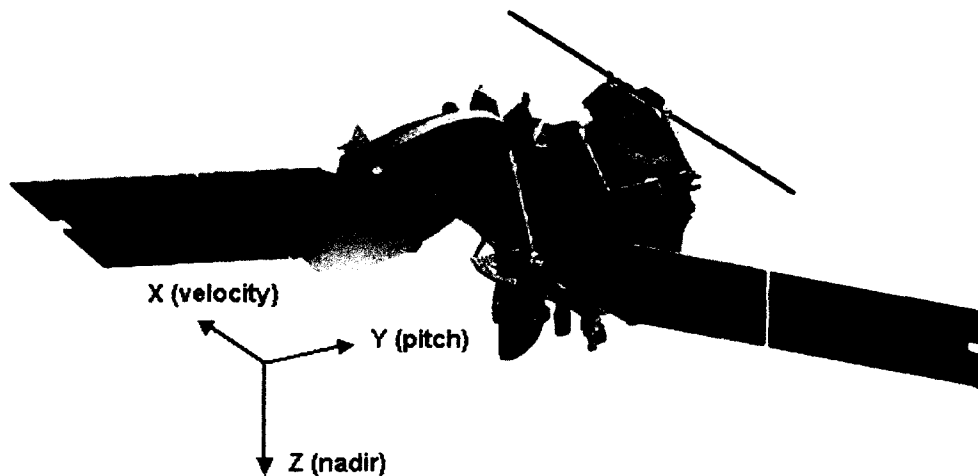


Figure 1 MRO Spacecraft Configuration in the Primary Science Orbit

HIRISE SCIENCE INSTRUMENT

The primary functional requirement of the HiRISE imager is to allow identification of both predicted and unknown features on the surface of Mars to a much finer resolution and contrast than previously possible. As such, the HiRISE instrument is the driver for MRO pointing and stability requirement.

HiRISE Design Features

The HiRISE instrument performance goals are listed in Table 1. The design features a 50 cm aperture and a detector with 128 lines of Time Delay and Integration (TDI).

| Parameter | | Performance | Comments |
|-------------------------------|------------------|--|--|
| Ground Sample Distance (GSD) | | 50 cm/pixel | From 400 km altitude 25 cm/pixel from 200 km |
| Telescope Aperture | | 0.5 m, f/24 | For resolution and SNR |
| SNR | Blue-Green | Typically 100:1 | Achieved with TDI, backside thinned CCDs, and 50 cm aperture |
| | Red | Typically 200:1 | |
| | NIR | Typically 100:1 | |
| Spectral range | | 400 to 600 nm 550 to 850 nm 800 to 1000 nm | Blue-Green (BG) Red NIR |
| Swath | Red | > 6 km | From 300 km altitude |
| | Blue-Green & NIR | > 1.5 km | From 300 km altitude |
| Swath length | | >2× swath width | Along track |
| Dynamic range | | 3,750:1 | Without binning, full well/system noise |
| Data Precision | | 14 bit A/D | 12 to 13 bit usable |
| Data Compression | | Real-time 14 to 8 bit | Look-up table |
| | | Up to 16 × 16 binning | Increases areal coverage |
| | | Felics compression at SSR | ~2 to 1 |
| Data storage | | 28 Gbits | All channels |
| Number of pixels across swath | | 20,264 4,072 | From swath width and pixel scale |
| TDI line time | | 76 μsec to 184 μsec | To match ground track speed |
| CCD read noise | | < 50 electrons rms at 10°C | Achieve SNR at low signal levels |
| FOV | | 1.14° × 0.1° | |
| IFOV | | 1 × 1 μrad | Detector angular subtense |
| Relative Radiometry | | <1 % pixel to pixel | Absolute 20% |

Table 1 HiRISE Requirements and Performance Characteristics

The imager design is an all-reflective telescope with light-weighted Zerodur optics and a graphite-composite structure. The slightly off-axis Cassegrain objective with relay optics is optimized for diffraction-limited performance over the long, narrow field-of-view (FOV) required for “push-broom” scanning and imaging. Filters in front of the detectors provide images in the three wavelength bands: red (or panchromatic), blue-green (BG), and near infrared (NIR).

The detector-chip-assemblies (DCA) housing the CCDs are staggered to provide full swath coverage without gaps. Both the BG and NIR bands have two DCAs each to give a total swath width of 4072 pixels, and the red channel has ten DCAs to give a much larger swath width of 20,264 pixels.

HiRISE features a 50 cm diameter primary mirror. For compactness a relay optical section follows the F/8 Cassegrain telescope giving a system focal ratio of F/24 at the focal plane. The HiRISE optical system meets the science requirements by providing a 30-cm per pixel diffraction limited MTF on 12 μm pixels for all 14 HiRISE detectors. The HiRISE color filters are located 40 mm from the detectors for all three channels. This distance avoids problems due to stray light and multiple reflections from the filters in the F/24 quasi-collimated beam. A Lyot stop, located between the last fold mirror and the tertiary mirror, ensures excellent stray light control.

Distortions in the large field of the panchromatic channel have been analyzed. As HiRISE points in the image of the Mars’ surface track along each CCD column in TDI mode, a point in the image will remain in a single CCD column with no cross column smear for all HiRISE detectors.

The HiRISE telescope structure is made of graphite-fiber-reinforced composite. This produces a stiff, lightweight structure with low moisture absorption properties and low coefficient of moisture expansion. The coefficient of thermal expansion (CTE) of the composite elements, in conjunction with metallic fittings, is tailored to produce near-zero CTE. Figure 2 shows the full-size model of HiRISE.



Figure 2 Full-size Mockup of HiRISE (Approximately 70 cm in Diameter by 1.4 m in Length)

HiRISE Focal Plane Subsystem

The FPS consists of DCAs, a focal plane substrate of aluminum-graphite composite material, a spectral filter assembly, and CCD processing/memory modules (CPMMs). Each DCA holds a single line scan CCD, with 2048 12×12 um pixels in the cross-scan direction and 128 TDI elements (stages) in the along-track direction. The 14 staggered DCAs overlap by 40 pixels at each end of each CCD as shown in Figure 3. This provides an effective swath width of 20,000 pixels for the panchromatic images and 4,072 pixels for the blue-green and NIR images.

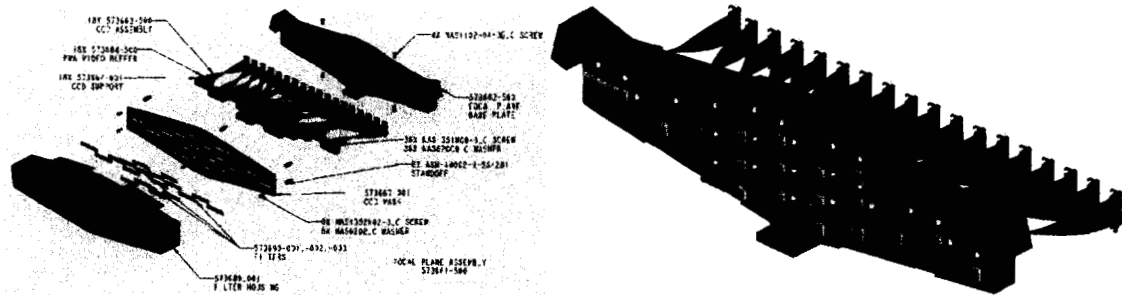


Figure 3 Focal Plane Assembly (left) and Focal Plane Layout of Detector Chip Assemblies (right)

Using the TDI method increases the exposure time, allowing us to obtain both very high resolution and a high signal-to-noise ratio. As the spacecraft moves above the surface of Mars, TDI integrates the signal as it passes across the CCD detector by shifting the accumulated signal into the next row (line) of the CCD at the same rate as the image moves (see Figure 4). The line rate of 13,000 lines/sec corresponds to an integration time of 78 microsec for 300 km altitude. The pixel integration time is set to match the ground velocity so that charge from one image region is sequentially clocked into the next corresponding element in the along-track direction. The imager can use 8, 32, 64 or 128 TDI stages (detector elements in the along-track direction) to match scene radiance to the CCD full well capacity. Spacecraft orientation will compensate for image smearing during the integration period. A practical limit is reached when residual image smear and spacecraft pointing jitter seriously degrade the required resolution. The 128 lines is the largest number of lines that meets all requirements. Images with higher SNR and lower resolution images will be obtained by binning the signal from adjacent lines and pixels within the CCD, up to a maximum of 16×16 pixels.

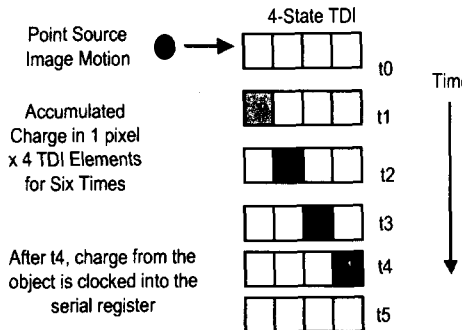


Figure 4 TDI Operation Using a 4-TDI Configuration to Illustrate Charge Accumulation

HiRISE Performance

The maximum signal is 76,000 electrons for the red channel at 300 km with no binning. Figures 5 and 6 show the expected un-binned SNR capability as a function of spacecraft latitude and regional albedo for the blue-green, red (pan) and NIR bands. Figure 7 shows end-to-end system level MTF curves for HiRISE at three levels of spacecraft jitter.

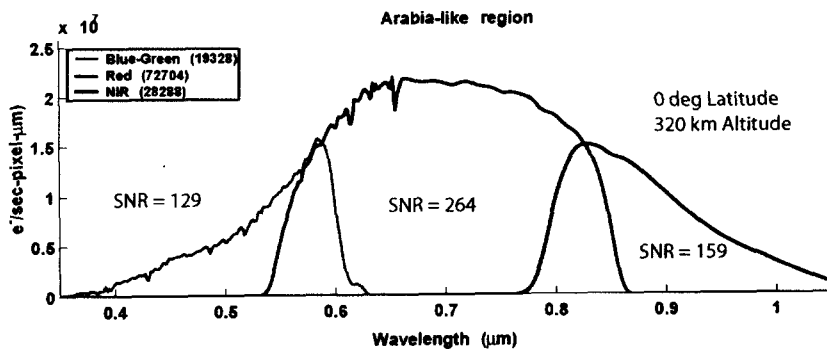


Figure 5 Signal in Electrons as a Function of Wavelength for a Bright Region of Mars

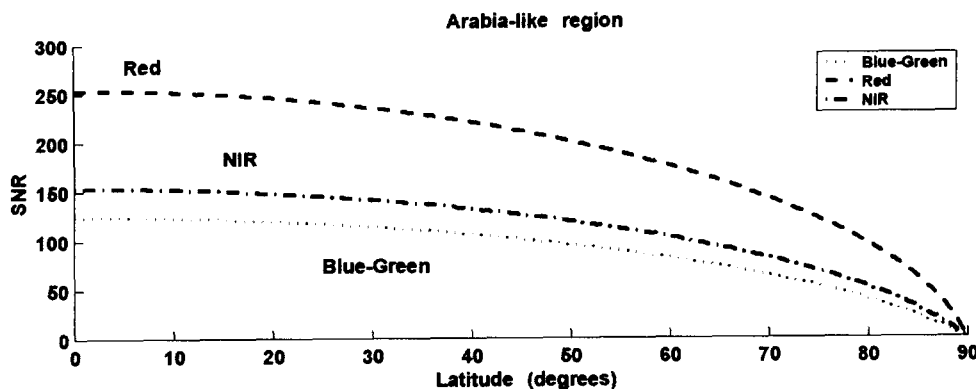


Figure 6 SNR for a Bright Region of Mars

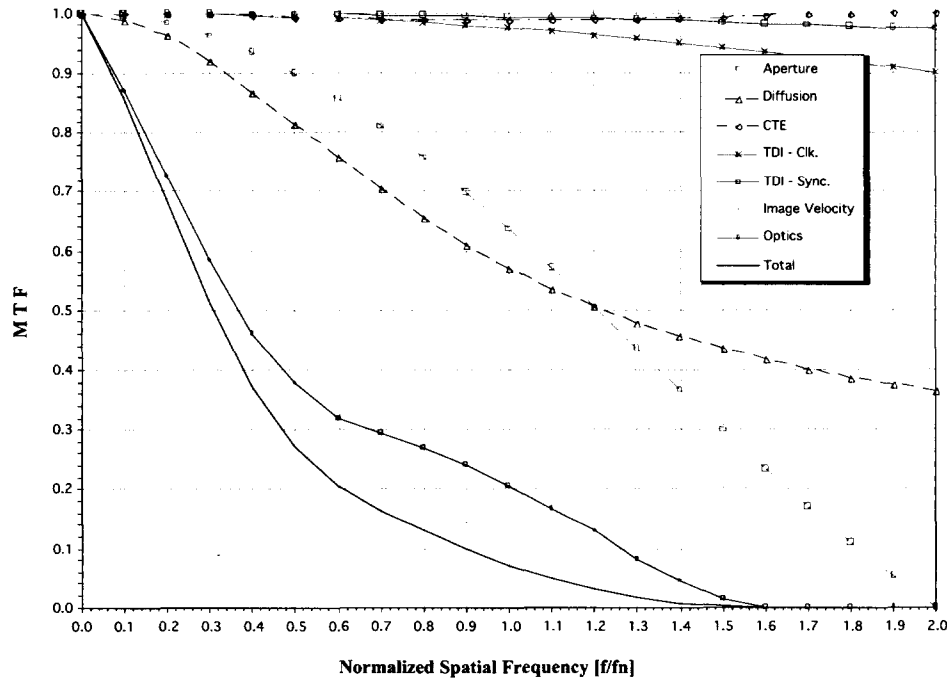


Figure 7 The diffraction limit of the telescope dominates the MTF

MRO GUIDANCE AND CONTROL

Pointing Performance-Related Requirements

Two types of pointing performance requirements drive the design of the MRO Guidance and Control Subsystem. The first type, target relative pointing, specifies how well a body-fixed vector must point at a target on the surface of Mars. The second type, pointing stability or jitter, specifies how still the spacecraft must remain (inertially) over a specified period of time.

Target-relative pointing requirements were levied on MRO by each imaging instrument. However, we only describe the HiRISE requirements because these are, by far, the most challenging. The fundamental HiRISE target-relative pointing requirements are:

- The HiRISE boresight shall point to a target on Mars to within 0.7 mrad (3-sigma) in the HiRISE FOV cross-track direction and 2 mrad (3-sigma) in the HiRISE FOV down-track direction.
- AND-
- The projection of the HiRISE instrument focal plane detector array onto the planet's surface is aligned perpendicular to the spacecraft direction of motion within 1 mrad (3-sigma) during HiRISE image acquisition.

The first target-relative requirement ensures that the target is captured in the instrument field of view. As described below, this requirement has implications for navigation accuracy, target location uncertainty, and spacecraft inertial pointing accuracy. The second requirement is necessary to minimize image smear.

Pointing stability requirements ensure that the image quality meets the science objective. As mentioned above, pointing stability refers to the allowable spacecraft rotational motion over a specified period of time. As with the target-relative pointing requirements, the HiRISE stability requirements are the most challenging of all the pointing stability requirements; however, in Table 2 we list each instrument's pointing stability requirements.

| Instrument | Magnitude | Window |
|------------|-------------|----------|
| HiRISE | 0.0032 mrad | 12 msec |
| CTX | 0.020 mrad | 1 msec |
| CTX | 0.020 mrad | 2.5 msec |
| CRISM | 0.032 mrad | 200 msec |
| ONC | 0.033 mrad | 300 msec |
| CRISM | 0.107 mrad | 1 sec |
| MCS | 1 mrad | 2 sec |
| MCS | 3 mrad | 16 sec |

Table 2 MRO Science Instrument Pointing Stability Requirements

GN&C Subsystem Description

The G&C hardware suite and the component locations on the spacecraft are shown in Figure 8. The subsystem consists of two Honeywell Miniature Inertial Measurement Units (MIMU), two Galileo Avionica A-STR star trackers, and four Honeywell Constellation Series HR16 reaction wheels. The A-STR star trackers provide attitude quaternion estimates at 10 Hz. The MIMUs utilize three orthogonal ring laser gyros to provide angular rate data at 200 Hz.

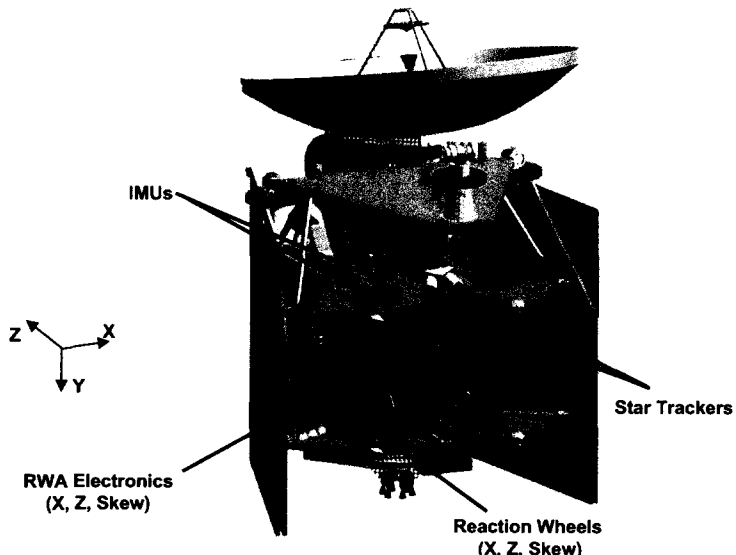


Figure 8 GN&C Subsystem Hardware Configuration

Attitude estimation is performed by a 6-state Extended Kalman Filter,^{**5} which combines attitude quaternion estimates from the star tracker with angular rate measurements from the inertial measurement unit to produce a 3-state attitude error estimate and 3-state gyro bias estimate. Ground-generated ephemeris and pointing commands are uploaded to the spacecraft, which uses them to construct an attitude command.

Pointing Strategy

Unlike Earth-based imaging spacecraft designed around a single high-resolution sensor,^{**6, **7, **8} the Mars Reconnaissance Orbiter will provide science observations from multiple science sensors. Therefore, many of the design optimization approaches applied to these Earth-based spacecraft simply cannot be applied to the MRO design. Specifically, the MRO spacecraft must be designed to support continuous nadir-oriented science operations at Mars, with periodic maneuvering to acquire high-resolution images of ground-specified targets. Although the MRO pointing accuracy and stability characteristics must support the

HiRISE instrument requirements, they cannot be accomplished without regard to operations of the other instruments, or without regard to the power and telecommunications constraints of Mars-orbital operations. Unlike their Earth-based brethren, MRO must provide precision-pointing capability while operating multiple instruments (some of which include gimbaled platforms), and while providing solar array and high-gain antenna tracking. Adding to the design challenge, the MRO spacecraft is a relatively large spacecraft bus (> 1000 kg for start of science operations), has large articulated appendages with low-frequency structural modes (< 1 Hz), and has a large fuel load with very low frequency slosh modes (< 0.01 Hz). These characteristics limit the agility of the MRO spacecraft needed to achieve targeted surface imaging.

Because of its narrow field of view and extremely high resolution, the HiRISE target-relative pointing and jitter requirements are the most challenging of all the instruments. To this end, the spacecraft will point the calibrated HiRISE boresight at the imaging target during the primary science phase, with the other instrument teams accepting the misalignment between the HiRISE boresight and their instrument's boresight as part of their pointing error budget. One complication associated with TDI-type imagers is the image smear seen if the target apparent motion is not aligned with the image scan direction. For a nadir-pointed vehicle such as MRO, the target apparent motion is a combination of the spacecraft orbital motion and the rotational motion of the planet. Since the HiRISE boresight is nominally aligned with the spacecraft yaw axis, a small yaw offset can be added to the nominal nadir-pointing attitude to eliminate smear. For MRO, this yaw offset can be as large as 5 deg (at the equator).

Target-Relative Pointing Budget

As a TDI instrument, HiRISE requires control of the boresight direction to capture the target in the field of view as well as rotational control about the boresight for smear compensation. The primary HiRISE pointing error sources are listed in Table 3 followed by a brief description of each error.

| Error Source | Magnitude (all values are 3-sigma) |
|--|---|
| Inertial Attitude Accuracy (calibrated HiRISE boresight) | 0.7 mrad about X, 1.0 mrad about Y and Z |
| Predicted Ephemeris Uncertainty | 1.5 km in-track, 0.5 km cross-track, 0.04 km radial |
| Spacecraft Clock Error | 10 msec |
| Target Horizontal Position Uncertainty | 600 m per axis |
| Surface Altitude Uncertainty | 500 m |

Table 3 Target Relative Pointing Error Sources and Allocations

Inertial attitude accuracy is the accuracy to which the spacecraft can orient a body-fixed reference frame in inertial space, and it includes control errors as well as inertial attitude determination uncertainty (for MRO, the body-fixed reference frame is assumed to be the HiRISE calibrated boresight). This allocation becomes a requirement levied on the spacecraft design team.

MRO measures (via the star tracker) its inertial attitude; it has no Mars-relative attitude sensing capability. To point a body-fixed vector at a target on the surface of Mars, knowledge of the spacecraft position with respect to Mars is required. Updated spacecraft ephemerides will be uplinked to the spacecraft every 48 to 72 hours, with maximum ephemeris uncertainty occurring just prior to uplink (and assumed in the pointing budget). Incidentally, the in-track ephemeris uncertainty is by far the largest contributor to the target-relative pointing budget. This allocation becomes a requirement levied on the Navigation team.

Errors in the onboard spacecraft clock have two effects on spacecraft pointing: for a given time they result in an error in the knowledge of the spacecraft in-track position and an error in the knowledge of rotational position of Mars. This allocation becomes a requirement on the operations team to calibrate spacecraft clock drift.

The final two error sources are simply caused by our inexact knowledge of Mars geography. Target horizontal position uncertainty is the uncertainty in the target location on the surface of Mars. For targets that are not directly below the spacecraft, surface altitude uncertainty results in a pointing error.

Pointing Stability Budget

The HiRISE pointing stability tree is shown in Figure 9, which illustrates and categorizes the disturbances and error sources that affect pointing stability. Figure 10 provides an illustration of how these errors affect image quality for the HiRISE TDI imager. The low-frequency disturbances from sources such as control loop rate error, uncompensated IMU bias, flexible body dynamics, propellant slosh, etc, affect image quality because they result in motion of the HiRISE boresight across the TDI columns. These *rate errors* are combined in a root-sum-square sense because they are uncorrelated and all appear as roughly constant over the imaging window time period. *Jitter sources*, on the other hand, generally have distinct spectral components of at least 20 Hz and, as such, are added within the pointing stability budget. The largest jitter sources for MRO are due to reaction wheel imbalance, the CRISM cryocooler, and the HGA gimbal drives (the solar array gimbals, as explained in the following section, are paused during high-resolution imaging). Finally, *misalignments* between instruments and sensors also result in an error in the target direction of motion through the field of view, so these are also included in the pointing stability budget and are combined in an RSS sense.

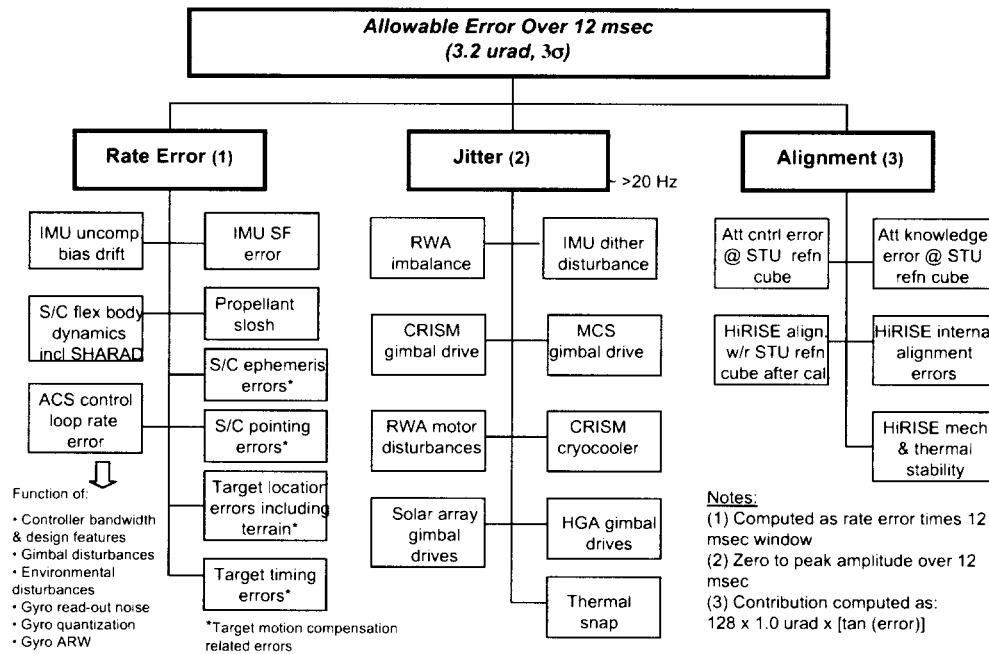


Figure 9 HiRISE Pointing Stability Tree

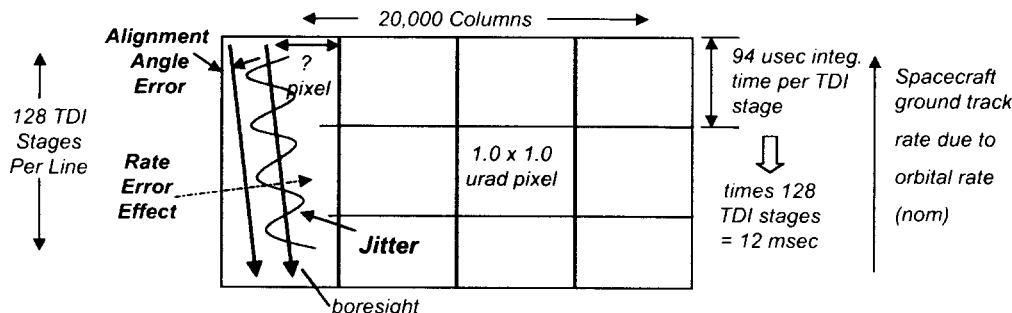


Figure 10 Effect of Jitter, Rate Error, and Misalignment on HiRISE TDI

The pointing stability budget for a 12 msec window is shown in Table 4 (12 msec corresponds to the maximum time window in the HiRISE pointing stability requirement). Among the rate error components, ACS control loop rate error is by far the largest contributor at 0.6 microrad, though this is relatively small compared to the overall budget of 3.2 microrad. Among jitter sources, reaction wheel imbalance, the CRISM cryocooler, and the HGA gimbal drive dominate the budget. It is interesting to note that, because of the low-frequency content of slosh disturbances relative to most of the stability requirement windows, slosh has been determined to be a insignificant contributor to stability performance. Strategies for managing the contributions of these disturbances are described in the following section.

| Error Category/Term | Allocation (microrad) |
|--|-----------------------|
| IMU Uncompensated Bias Drift | 0.02 |
| IMU Scale Factor Error | 0.01 |
| S/C Flexible Body Dynamics (including SHARAD) | 0.07 |
| Propellant Slosh | 0.05 |
| Target Location Errors (including terrain) | 0.01 |
| Target Timing Errors | 0.09 |
| S/C Ephemeris Errors on Motion Compensation | 0.02 |
| S/C Pointing Errors on Motion Compensation | 0.01 |
| ACS Control Loop Rate Error | 0.60 |
| RWA Imbalance | 1.25 |
| IMU Dither Disturbance | 0.27 |
| CRISM Gimbal Drive | 0.10 |
| RWA Motor Disturbances | 0.13 |
| CRISM Cryocooler | 0.63 |
| HGA Gimbal Drives | 0.57 |
| Thermal Snap | 0.00 |
| MCS Gimbal Drive (gimbal motion assumed paused) | N/A* |
| Solar Array Gimbal Drives (gimbal motion assumed paused) | N/A* |
| Attitude Control Error w.r.t. Star Tracker | 0.10 |
| Attitude Knowledge Error w.r.t. Star Tracker | 0.10 |
| Calibrated HiRISE Alignment w.r.t. Star Tracker | 0.08 |
| Calibrated HiRISE Internal Alignment | 0.08 |
| HiRISE Mechanical and Thermal Stability | 0.04 |

Table 4 – HiRISE 12 msec Pointing Stability Allocation

MRO DISTURBANCE SOURCES

The following discussion presents the design approach undertaken to address MRO-unique issues. The major error sources shown in the pointing stability allocation are discussed, along with their mitigations. Included are the gimbaled science platforms (MCS and CRISM), the CRISM cryogenic cooler, the solar array and high-gain antenna articulation, the reaction wheel imbalance and related desaturation strategy, and disturbances from the dither of the IMU's ring-laser gyro assembly.

Analysis Approach for Pointing Stability Requirements

Analysis of MRO's many pointing accuracy and stability requirements reveals the HiRISE requirements to be the most stringent, and establishes them as the principal design drivers. In this context, the approach taken to meeting MRO pointing accuracy and stability requirements has been to design to the HiRISE requirements, and then verify that the other pointing stability requirements are met as well. This approach has generally proven successful, although some design tweaks have been needed even after meeting all the HiRISE requirements.

The jitter and rate error contributors have been evaluated using various methods. Jitter was evaluated by first building a NASTRAN Finite Element Model (FEM), as shown in Figure 11, and then modeling the transmissibility of the various disturbances to the HiRISE mounting base. Typical and worst-case disturbance sources were analyzed and time histories created. The disturbance sources examined include stationary sources (reaction wheel imbalance, cogging, and ripple, IMU dither, CRISM cryocooler, gimbal DC motors, and MCS stepper motors) and transient sources (harmonic drive irregularity of the solar array and high-gain antenna gimbals, CRISM scan torque profile, and MCS scan torque profile). For the MRO analysis, jitter motion consists of dynamics higher than 20 Hz. Low-frequency motion, which shows up as essentially a rate-tracking error, has been analyzed with a combination of closed loop simulations, Monte-Carlo assessments and analytical tools. For the MRO analysis, low-frequency motion consists of dynamics less than 10 Hz.

The results of these assessments have been provided to the instrument providers, allowing them to assess their requirements and refine them as appropriate. For high-frequency jitter, the instrument providers were given time histories of crosstrack and downtrack motion. Data was provided for a 10 sec window with 10 microsec time steps. A single rate error value containing the combination of all of the low frequency components was also provided.

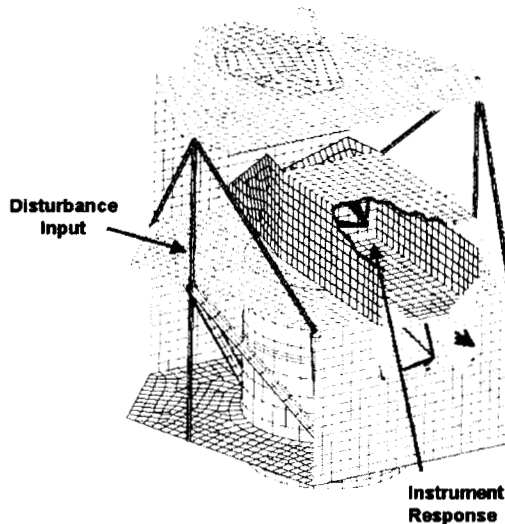


Figure 11 MRO Core Spacecraft FEM

The instrument providers reviewed and analyzed the data, and provided their evaluations. Ball examined the data in great detail, using their “TRADES” simulation tool to generate TDI image lines for relative evaluation of image quality. Based upon their assessment, several instrument stability requirements were revised and some spacecraft design changes were made to improve performance. These changes included stiffening all deck structure by increasing deck core and face sheet thickness, and redesigning the optical bench to accommodate HiRISE mounting and isolate it as much as possible from solar array and HGA gimbals. Several operational changes were also made, including “freezing” the solar array gimbals and the MCS scan platform during high-resolution imaging. The following discussion provides more detail on why these changes were needed.

Other Science Instruments (CRISM and MCS)

As discussed earlier, the MRO spacecraft must support simultaneous operations of multiple science instruments. Spacecraft disturbances from two instruments are of particular concern for high-resolution imaging, these instruments being CRISM and MCS. Both of these instruments have gimbaled platforms and the CRISM instrument design includes a cryocooler. The MRO science mission includes “coordinated observations” between HiRISE and CRISM, so CRISM must be able to operate during these high-

resolution imaging periods. However, the MCS science collection is independent of the HiRISE instrument, and so could be interrupted for brief periods if necessary.

Representative disturbance profiles from the CRISM and the MCS instruments are shown in Figure 12. These profiles were constructed based upon typical scan motion profiles of both instruments and their respective dynamics models. As can be seen from these profiles, the MCS torque disturbances are roughly an order of magnitude worse than the torque disturbances from the CRISM instrument.

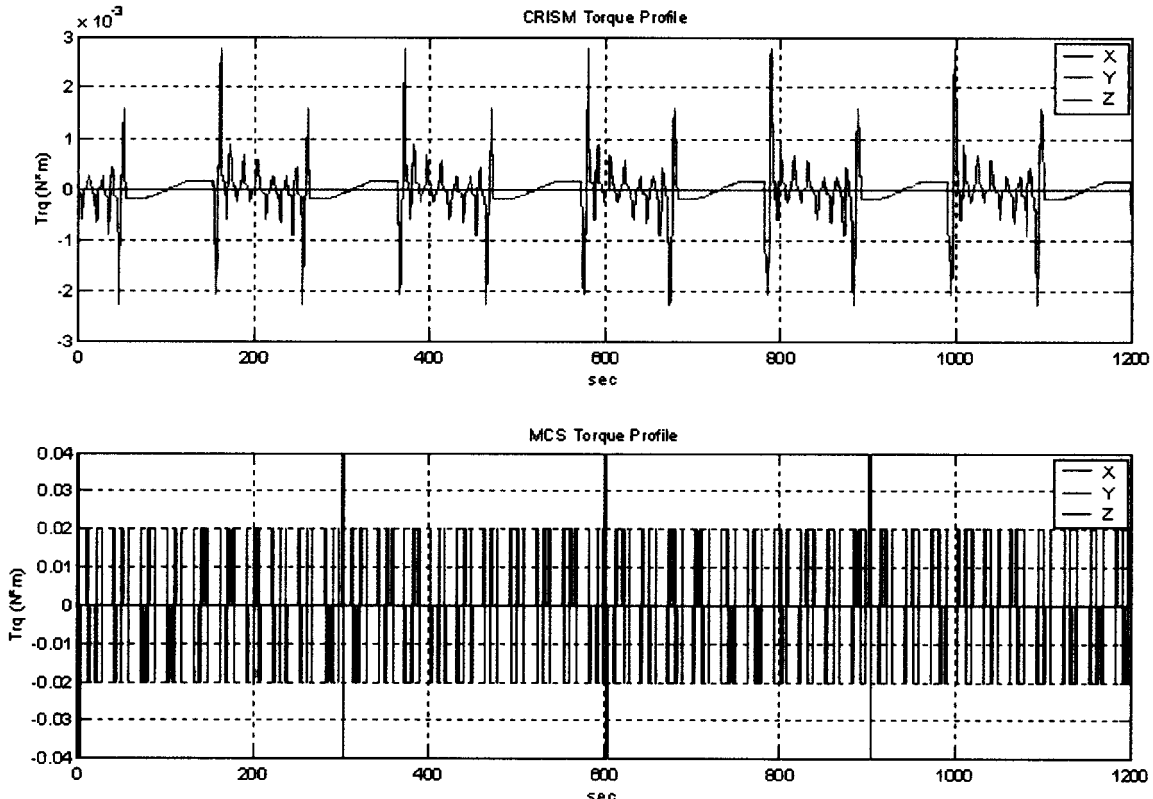


Figure 12 - Representative CRISM and MCS Gimbal Torque Profile

An orbital simulation for MRO has been run with the above disturbance profiles to assess the pointing stability impacts. A preliminary design of the flight control laws was included in the simulation which has a bandwidth of approximately 0.1 Hz. To isolate the effects of the payload gimbal motion, no other gimbals were running (e.g., the solar arrays and the high-gain antenna were fixed in a nominal position). Additionally, the environmental disturbance models were disabled for this simulation. Representative structural models and slosh models were included, with the first structural mode at 1.08 Hz and the zero-g slosh mode at 0.007 Hz; the simulation results are shown in Figure 13. Because the payload disturbance torques have significant energy above the bandwidth of the controller, the simulation shows significant motion of the spacecraft (peak amplitude of approximately 35 microrad).

The gimbal design also includes a fairly large gear reduction (260:1) implemented with a harmonic drive. Although harmonic drives are efficient mechanisms from a mass perspective, they have many undesirable dynamics characteristics for a precision-pointing spacecraft. Chief among these is the nonlinear and position-dependent friction characteristics. The MRO design attempts to limit the friction effects by implementing a tight control loop (20–30 Hz bandwidth) on the gimbal rate. However, this effort involves instead developed based upon the gimbal development efforts. The initial MRO analysis, which instead have been assumed to be quite conservative.

Odyssey's spacecraft data.¹⁰ Although the MRO motor design is quite different from Odyssey's motor design (Odyssey uses stepper motors), the harmonic drive design is similar. Therefore, the gimbal model development work and the performance goals have been proven. For the initial MRO analysis, minimal improvements have been assumed to be quite conservative. The initial MRO analysis, which instead have been assumed to be quite conservative.

Odyssey's spaceflight observations of articulation disturbances from 2001 Mars Global Surveyor also indicate that the gimbal error is significantly reduced by using a Hall-effect sensor instead of a simple Hall-effect switch. This allows a position-dependent current command, rather than a simple Hall-effect scheme, to reduce the motor cogging.

Because the MRO solar array and high-gain antenna are very large, they represent significant disturbance sources during tracking. The gimbals have been carefully designed to eliminate the motors as a significant vibration source. The gimbal design utilizes a DC brushless motor, rather than a more traditional stepper motor, to eliminate the disturbance associated with stepper motors. Furthermore, the commutation of the DC brushless motor is implemented using synchronous resolvers instead of Hall-effect sensors. This allows a position-dependent current command, rather than a simple Hall-effect switch.

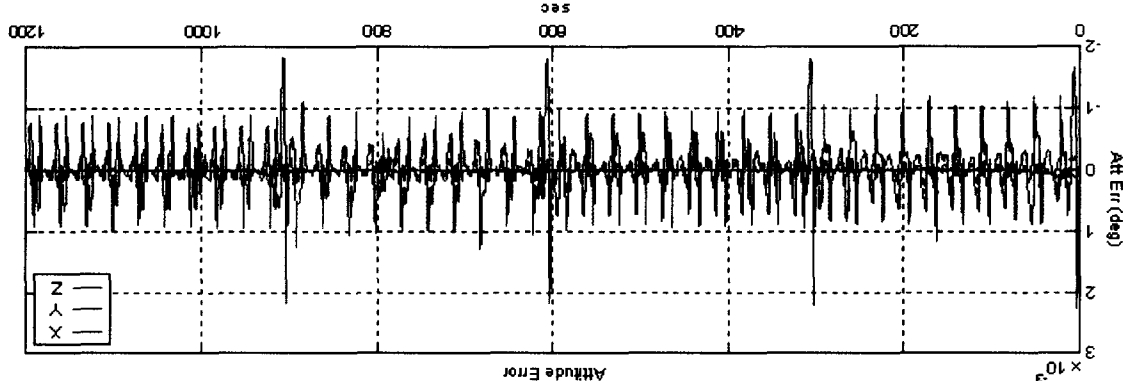
Solar Array and High-Gain Antenna

Because the CRISM instrument's stirring cryocooler and gimbal disturbances on HIRISE bore significant stability. Therefore, the CRISM instrument has been located as far from HIRISE as possible to reduce cryocooler vibration. The CRISM instrument has been located as far from HIRISE as possible to eliminate cryocooler vibration. Therefore, the CRISM instrument has been located as far from HIRISE as possible to reduce cryocooler vibration.

Another significant payload disturbance source is the CRISM instrument's stirring cryocooler. Because of the high resolution and relatively long integration time of the HIRISE instrument, the high-frequency vibration of a cryocooler can easily violate HIRISE pointing stability requirements. The MRO Science vibration resolution of a cryocooler can easily violate HIRISE pointing stability requirements. The HIRISE and CRISM instruments require that HIRISE and CRISM perform coordinated observations of Mars surface targets, and therefore it would be desirable to have them co-located to achieve the best possible co-alignment. However, co-locating HIRISE and CRISM on the same deck would exacerbate the CRISM cryocooler microphonics effect upon HIRISE. Analysis of cryocooler data provided by Johns Hopkins Applied Physics Lab (APL)¹¹ shows the need for significant structural attenuation of the microphonics effect upon HIRISE and CRISM on the same deck would exacerbate the CRISM cryocooler vibration. The CRISM instrument has been located as far from HIRISE as possible to reduce cryocooler vibration.

Detailed analysis of the attitude data shown in Figure 13 indicates that most of the motion is caused by the

Figure 13. Spacecraft Attitude Error Response to CRISM & MCS Gimbal Motion



A Mars orbital simulation was constructed in ADAMS/Simulink to analyze the low-frequency, transient dynamics resulting from solar array and high-gain antenna gimbal motion, as well as from CRISM and MCS gimbal motion. The simulation incorporates moderately high-fidelity models, including a full reaction wheel control model for the spacecraft, a full gimbal control model for the solar array and high-gain antenna, and representative CRISM and MCS disturbance profiles. The spacecraft model consists of an FEM structural model, including structural modes for the solar arrays, compliant gimbals for the solar array and the high-gain antenna, and Odyssey-like harmonic-drive disturbances.

Some simulation results from this model are presented in Figure 14, showing significant stability excursions above HiRISE requirements. Because of these simulation results, an operational constraint has been imposed to stop solar array gimbal motion during high-resolution imaging. Although stopping motion of the high-gain antenna could produce some additional stability gains, HGA motion does not violate the stability requirements and the desire to maintain communications throughout high-resolution imaging outweighs the desire for improved stability. The simulation results have also led to some minor structural design changes to improve HiRISE pointing stability. The gimbal support deck was modified to take disturbances down struts to core cylinder, thereby reducing the transmissibility of vibration from the gimbals to HiRISE.

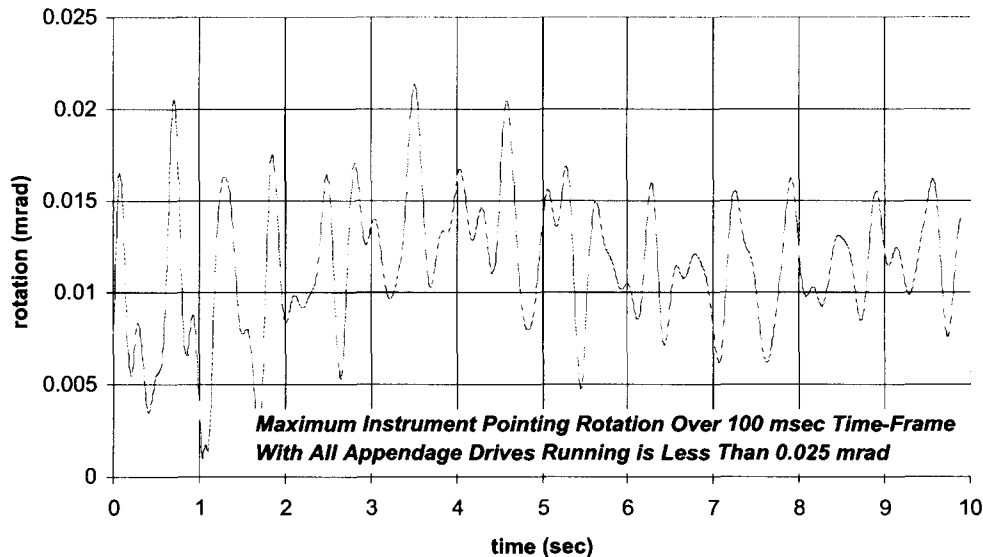


Figure 14 MRO Pointing Stability Simulation Results (Maximum Deviation over 100 msec) including Solar Array, HGA, CRISM, and MCS Gimbal Motion

Reaction Wheels and Inertial Measurement Unit (IMU)

Both the reaction wheels and the inertial measurement unit (IMU) can be significant vibration sources, and can adversely affect pointing stability for high-resolution imaging. Each reaction wheel has its own static and dynamic imbalance that produce vibration when spinning. Because the vibration magnitude is proportional to the square of the speed, better pointing stability can be achieved by operating the reaction wheels at lower speeds. Therefore, large momentum-capacity reaction wheels and frequent desaturation events would optimize pointing stability. For the MRO spacecraft, the Navigation team has imposed a maximum desaturation frequency of one desaturation event every 48 hours to meet orbit prediction accuracy requirements. Therefore, design flexibility is only available in reaction wheel sizing and balancing. A large capacity off-the-shelf wheel size (100 N-m-s) has been selected for MRO, which provided the best trade-off between momentum capacity and wheel balancing. Extra balancing activities are required for MRO to minimize reaction wheel vibration over the operational speed range. To further limit the effect of wheel vibration on HiRISE stability, the wheels have been placed as far away from the HiRISE optical bench as possible.

The IMU selected for use on MRO contains three ring laser gyros (RLGs), which are dithered to improve performance at low rotation rates. The dither frequencies are in the range of 400 to 700 Hz. The IMU can either be procured with the RLGs internally isolated from the chassis, or without internal isolation. Without internal isolation, relative alignment knowledge between the star tracker and the gyros can be improved by more than an order of magnitude. This can help pointing accuracy when slews to a surface target are required. However, removing the internal isolation greatly increases the dither vibration observed at the IMU mounting interface, which can degrade pointing stability. For MRO, this has been resolved by imposing an operational constraint on targeted imaging. Each off-nadir targeted slew must have time allocated to star acquisition following the slew, which removes the need for extremely tight IMU to star tracker alignment knowledge. This allows MRO to include internal isolation in the IMU, which improves pointing stability.

Simulation results of crosstrack jitter are shown in Figure 15. In this figure, we have zoomed in to show the time-history details over 0.3 sec. Included in the simulation results are reaction wheel speeds of 1000, 2000, and 3000 RPM, with the static and dynamic imbalance numbers discussed above. The HGA is assumed to be articulating, but the solar arrays are frozen in a nominal orientation. The CRISM cryocooler is assumed to be operating. Finally, the IMU is assumed to be operating without any internal isolation. Although this is not the current baseline, it was analyzed this way to assess the worst-case scenario. As can be seen in the figure, reducing the reaction wheel speeds from 3000 RPM (blue) to 2000 RPM (green) significantly improves the jitter characteristics.

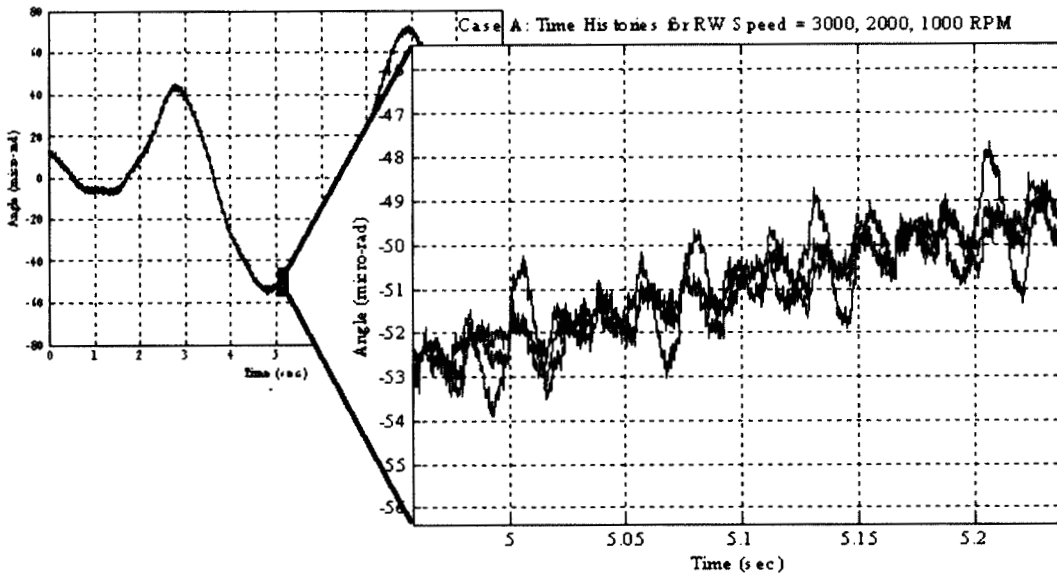


Figure 15 Simulated Time History of Crosstrack Jitter Response at HiRISE Mounting Interface

A detailed statistical analysis was performed on the jitter simulation results. The simulation was run for a number of cases; each case represents 10 sec of simulated motion, and results were output at 0.5 msec time steps. Various time windows were examined, with the most stressing time window being 12 msec. The 12 msec time window was passed over the 10 sec of simulation data to provide 20,000 distinct windows of 25 data points each. The mean (in microrad) for each window was computed, as well as the distance of each sample from the mean. Statistics for all 20,000 windows were then computed from these results.

A stressing case in which all three reaction wheels were spinning at 3000 RPM is shown in Figure 16. The left side of Figure 16 shows the jitter distribution, and the right side shows the cumulative distribution. From this figure we see that the jitter is less than 0.9 microrad approximately 94% of the time for this stressing case. The jitter is less than 0.5 microrad for approximately 72% of the time. These numbers are significant, because the HiRISE pixel width is 1.0 microrad. This means that, even for this bad stack up of

error sources and for the longest possible HiRISE integration time, a point source would stay within single TDI column 72% of the time.

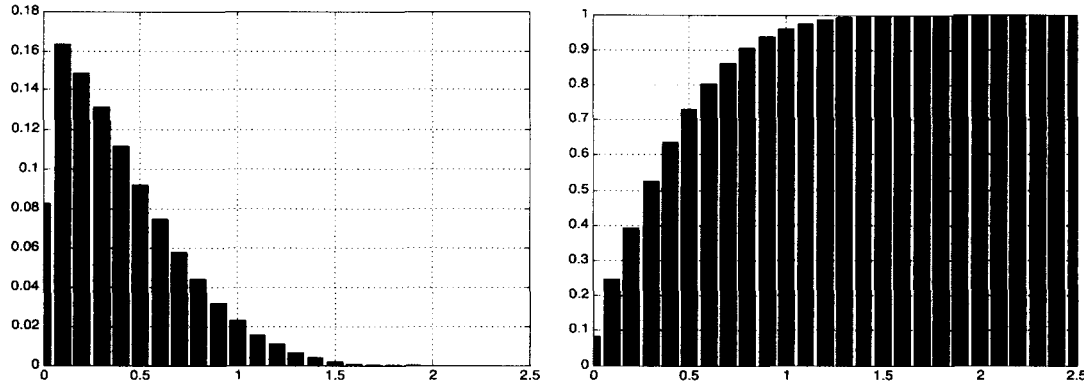


Figure 16 Jitter Distribution [left] and Cumulative Jitter Distribution [right] for 12 msec Imaging Period (RWA speed of 3000 RPM)

OVERALL ESTIMATED PERFORMANCE

A moderate-fidelity simulation was constructed to assess the MRO pointing accuracy and stability characteristics under the above assumptions. Pointing stability results of this simulation are shown in Figure 17. The startup transients die out within the first 100 sec of simulation time; the remainder of the simulation represents realistic pointing stability characteristics. As can be seen in the figure, the solar array motion produces unacceptably large disturbances for high-resolution pointing, even when the MCS gimbal platform is frozen. When the solar array is stopped (approximately 350 sec into the simulation), a transient is observed in the pointing stability followed by very good pointing stability. Without solar array motion, the simulation predicts that the HiRISE stability requirements will be met with significant margin. The simulations indicate that the pointing strategies will support the ambitious MRO science objectives, and that the various MRO science goals are achievable. Higher-fidelity simulation models will become available as the MRO design matures, and the pointing accuracy and stability characteristics will continue to be closely scrutinized.

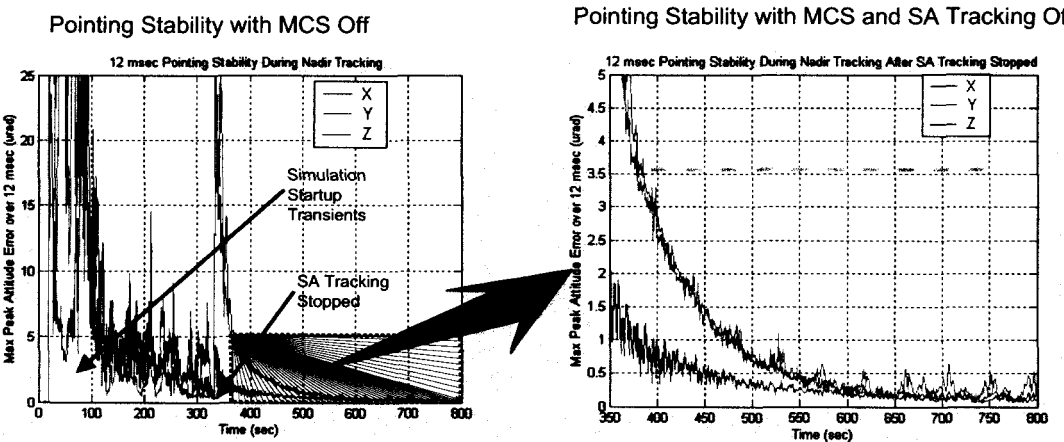


Figure 17 12 msec Stability Initial Results for HiRISE

CONCLUSION

In 2005 the Mars Reconnaissance Orbiter spacecraft will embark on its ambitious journey to explore Mars. The spacecraft will carry an impressive array of instruments including HiRISE, a high-resolution imager that will obtain stunning new images of Mars with a resolution of 50 cm/pixel. Producing such images, however, requires extremely tight target-relative pointing accuracy and stability capabilities; the precision required is unmatched by any previous interplanetary spacecraft mission. Although the nature of the MRO mission does not allow the spacecraft design to be optimized for high-resolution imaging, the design compromises discussed in this paper still produce an extraordinarily-capable vehicle. Analysis and simulation results indicate the MRO design will meet performance goals the vast majority of the time, with exceedances only under the most challenging combinations of error sources. The resulting design will allow exciting new discoveries as we continue to expand our knowledge of the planet Mars.

ACKNOWLEDGMENTS

This work was supported by the Mars Reconnaissance Orbiter program under contract to the Jet Propulsion Laboratory (contract number 1234906). Many thanks go to the many engineers at the Jet Propulsion Laboratory, Lockheed Martin, and Ball Aerospace who participated in the MRO pointing stability special study. Special acknowledgement is given to Dr. Phillip Good and Jason Wynn, who worked diligently in developing the MRO stability analysis techniques. Many others contributed in various ways through MRO program workshops and tabletop reviews, and helped developed a better understanding between instrument operations and spacecraft performance. The authors gratefully acknowledge all those who participated.

REFERENCES

- [1] "Mars Reconnaissance Orbiter Request for Proposal," California Institute of Technology Jet Propulsion Laboratory, RFP No. JPL-MRO-2005, Apr 2001.
- [2] Zurek, R., "Mars Exploration Strategy: Follow the Water," Keynote Presentation, 24th Annual AAS Guidance and Control Conference, Breckenridge, CO, Feb 2001.
- [3] Spath, S. R., and Eckart, D. F., "Fuel Optimization During Mars Global Surveyor Aerobraking," 23rd Annual AAS Guidance and Control Conference, Breckenridge, CO, Feb 2000.
- [4] Chapel, J. D., Johnson, M. A., Sidney, W. P., Willcockson, W. H., Wynn, J. A., Gulick, D., "Aerobraking Safing Approach for 2001 Mars Odyssey," 25th Annual AAS Guidance and Control Conference, Breckenridge, CO, Feb 2002.
- [5] E. J. Lefferts, F. L. Markley, and M. D. Shuster, "Kalman Filtering for Spacecraft Attitude Estimation," Journal of Guidance, Sep-Oct, 1982, Vol 5, No 5, p. 417.
- [6] Heffernan, P., and Martin, W., "Optimal Maneuver Control of a Precision Imaging Satellite," 26th Annual AAS Guidance and Control Conference, Breckenridge, CO, Feb 2003.
- [7] "DigitalGlobe Successfully Launches QuickBird Imaging Satellite," SpaceDaily.com, Oct 18, 2001.
- [8] "French Imaging Spacecraft Lofted into Polar Orbit by Ariane 4," Space.com, May 3, 2002.
- [9] Ross, R., "Critique of the Mars '05 CRISM Spectrometer Cryocooler Application—An Update," February 2002
- [10] Gehling, R., and Lynch, S., "Appendage Deployment Verification for the 2001 Mars Odyssey Spacecraft Using Spacecraft Attitude Telemetry," 26th Annual AAS Guidance and Control Conference, Breckenridge, CO, Feb 2003.